PREDICTING LIFETIME BEARING DEMANDS DUE TO BRIDGE AGING AND DESIGN VARIATIONS

PREDICTING LIFETIME BEARING DEMANDS DUE TO BRIDGE AGING AND DESIGN VARIATIONS

By

MINESH K. PATEL, M.Eng (Civil Engineering)

A thesis Submitted to the School of Graduate Studies in Partial Fulfilment of the Requirements for the Degree Master of Applied Science

McMaster University MASTER OF APPLIED SCIENCE (2019) Hamilton, Ontario (Civil Engineering)

TITLE: Predicting Lifetime Bearing Demands due to Bridge Aging and Design Variations

Author: Minesh K. Patel

Supervisors: Dr. Tracy C. Becker and Dr. Georgios P. Balomenos

Number of Pages: x, 51

ABSTRACT

The importance of long-term performance and safety of bridge bearings is paramount. Limitations in the inspection process as well as uncertainties in the maintenance scheduling of bridge bearings have led to a limited understanding of the lifelong performance of such components over their service life. To aid bridge owners facilitate an efficient system for repairs and management of bridge bearings, the initial step is to quantify the demands they typically experience over their service life. In this study, a framework quantifying bridge bearing demands due to thermal, traffic, and seismic loading is presented. The effect of bridge aging is accounted through corrosion prediction models. In reinforced concrete members, the reduction of the steel reinforcement and cover cracking and spalling is considered, and a uniform reduction of the steel in the case of steel members. Six bridge models are considered with variations in the number of bridge spans and two superstructure types; precast concrete girder and slab on steel girder. Monte Carlo simulation is used to account for uncertainties in corrosion model parameters and bridge loadings. The results of this study can be used for future experimental investigation of the fatigue performance of bridge bearings.

ACKNOWLEDGEMENTS

To my family, friends from across the globe, and the amazing people I have met along this incredible journey.

Thanks to the parents (Bio and Canadian) for their constant support along the way.

TABLE OF CONTENTS

TABLE OF FIGURES

LIST OF TABLES

LIST OF ALL ABREVIATIONS AND SYMBOLS

A	=	parameter related to environment and steel type (steel corrosion model)
B	=	parameter related to environment and steel type (steel corrosion model)
$C(t)$	=	average corrosion penetration at time t (steel corrosion model)
$C(x,t)$	=	chloride concentration as a function of depth x and time t
$C(x,t)$	=	chloride concentration as a function of depth x and time t
C_{cr}	=	critical chloride concentration
C_s	=	surface chloride concentration
D	=	diffusion coefficient (deck corrosion model)
d_{bi}	=	initial reinforcement diameter
$d_b(t)$	=	reinforcement diameter at time t
d	=	depth of concrete cover
D_0	=	diffusion coefficient (pier corrosion model)
E	=	Young's modulus
$erf(.)$	=	standard error function
h	=	depth of deck
I	=	second moment of area
k_c	=	curing factor
k_e	=	environmental factor
k_t	=	test method factor
M	=	applied deck moment
n	=	age factor
t_i	=	time to corrosion initiation (deck)
T_{corr}	=	time to corrosion initiation (pier and deck)
T_f	=	theoretical time when reinforcement diameter fully corroded
t_0	=	Reference time to diffusion D_0 (pier corrosion model)
$\frac{w}{c}$	=	water cement ratio
X_I	=	model uncertainty coefficient
α	=	thermal coefficient of expansion
ΔT	=	thermal gradient

1. INTRODUCTION

Bridge bearings are a key component of a bridge structure with the primary function of ensuring reduced forces throughout the structure by allowing displacement to occur in elements of high flexibility. Thus, bridge bearing maintenance is vital because failure of such components can lead to catastrophic consequences. Bearing failures can be categorized in several ways. Noury and Eriksson (2017) studied the failure mechanisms for high strength stainless steel roller bearings and showed corrosion induced cracking in combination with bearing fatigue is a primary cause and ultimately leads to failure. Cohen and Wetzk (2016) showed failures of rocker type bearings can be partly blamed due to the infrequency and lack of a thorough bearing maintenance and inspection process. Although bridges in Ontario are inspected every two years (Ministry of Transportation Ontario, 2019), visual inspection of bridge bearings can be a challenging task because parts of the bearing may not be visible. Further, the Bridge Condition Index (BCI) is an inspection method that helps to assess the condition of bridge elements, however the process is left to engineering judgement and it can be difficult to predict the remaining service life of such components. Therefore, uncertainties arise as to when bridge bearings may need repairing or replacing. Thus, to address the issues associated with bearing repair and replacement, it is first important to understand how they degrade over their service life.

Bridge loads such as daily traffic and temperature occur consistently over a bearing's service life and result in many bearing cycles occurring at small displacements. Many cycles over time lead to fatigue that causes some of the bearing properties to degrade. Warn and Deng (2016) showed that the stiffness of circular elastomeric bearings can be sufficiently reduced by fatigue induced cracking. Roeder et. al. (1990) experimentally investigated the fatigue effect on laminated elastomeric bearings and developed fatigue protocols under cyclic compression and shear which indicated that fatigue was heavily influenced by the range of strain and the rate of the applied loading. Yakut and Yura (2002) investigated elastomeric bearing behavior at low temperatures and showed that the shear stiffness can be severely influenced by temperature change because of the stiffening effect which occurs at low temperatures. This could have significant consequences to the bearings performance during colder months of the year. Therefore, the effects of fatigue can reduce a bearing's performance over time, and thus, quantifying bearing demands over the lifespan of the bearing will help to determine intervention times. The first step of this global framework is to quantify the bearing demands so that a loading protocol can be developed for future experimental investigation of bearing performance.

Canadian Highway Bridge Design Code (CHBDC) (CSA S6-2014) considers that the typical design life for new bridge structures is 75 years. During this lifespan, the condition of the bridge deteriorates through a process known as bridge aging.

For example, for reinforced concrete structures corrosion causes structural deterioration of the reinforcement over time, with two main processes being responsible for reinforcement deterioration (Zhou et. al. 2014):

- Carbonation: This is caused due to a reaction between the carbon dioxide present in the air and the concrete itself. Calcium carbonate is formed and this penetrates through the permeability of the concrete cover.
- Chloride Induced Corrosion: This is caused due to chloride ingress penetrating through the concrete cover and is typically quicker than the carbonation process.

Figure 1 shows a conceptual understanding of corrosion propagation with time. The initiation period is represented by T_{int} and it is the time taken for the chlorides or carbonates to pass through the concrete cover and interact between the steel and concrete interface, and then to initiate corrosion once the concentration of chlorides exceeds a threshold value. After corrosion is initiated, depassivation occurs whereby rust is formed due to the reaction between the chlorides and steel. This leads to tensile stresses developing and inducing cracks adjacent to the rebar, and finally causing spalling of the concrete cover as cracks propagate towards the surface. Figure Figure *1* shows the time to cracking and spalling of the cover concrete represented as T_{cr} and T_{spall} respectively.

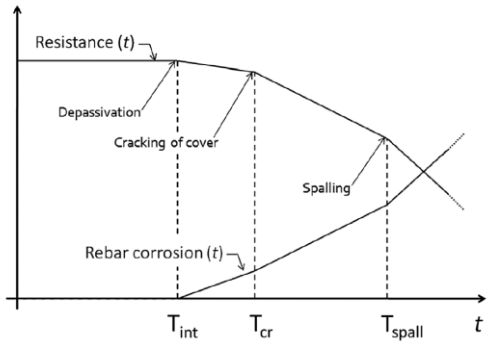

Figure 1. Corrosion initiation and propagation model in reinforced concrete (Rao et. al. 2016)

Aging of bridges is a significant issue, with over one third of the bridges owned by the Ministry of Transport Ontario (MTO) being over 50 years of age (Ministry of Transportation Ontario, 2019). Further, in Canada, over 40% of bridges are older than 50 years (Taylor and Brooks, 2013). Changes to the stiffness properties of the bridge due to aging can in turn influence the demands of the bridge components such as the bearings. Experimental investigations showed that flexural stiffness of individual reinforced concrete elements can be significantly reduced due to corrosion. For example, Torres-Acosta et al. (2004) tested reinforced concrete beams under accelerated corrosion for up to 180 days and showed that a 14% corrosion of reinforcement caused the flexural stiffness of the member to decrease by almost 33%. O'Flaherty et al. (2010) similarly found that 25% corrosion of the longitudinal reinforcement bars resulted in a 54% loss in beam stiffness due to an accelerated corrosion testing process. Kayser and Nowak (1989) investigated the structural reliability in the case of steel bridges due to general corrosion of the steel

girders. Stewart and Rosowsky (1998), and Vu and Stewart (2000) found that the effects of bridge aging for reinforced concrete decks has the potential to impact the structural reliability of these members, with the water cement ratio and deck cover to be the more influential parameters for the onset of corrosion. However, no research has investigated the effects of bridge aging on changes to the bearing demands over time.

In addition, there are several variations of bridge design parameters. For example, of the 2800 bridges owned by the Ministry of Transport Ontario (MTO), there is a significant variation in the numbers of spans of bridges as over 75% of these bridges are comprised of single, two or three spans (Figure 2). Also, precast concrete girder and steel girder bridges are the dominant types of superstructures.

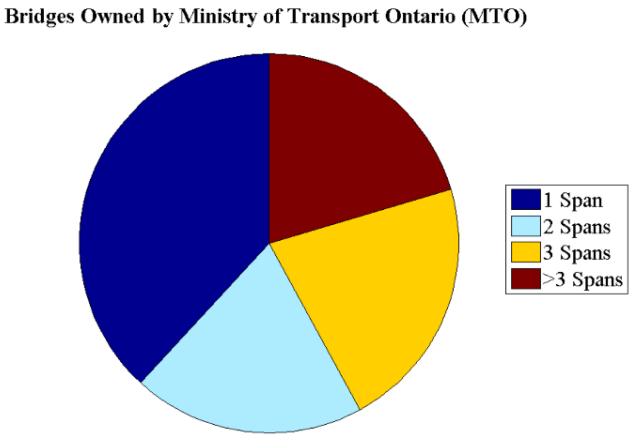

Figure 2. Variation in the number of spans of bridges owned by MTO (Ministry of Transport Ontario, 2019)

Noade and Becker (2019) quantified annual bearing demands over its service life considering three primary load types (temperature, earthquake and traffic). Traffic loading was shown to produce the largest number of cycles at low amplitudes of the design displacement of the bearing. Temperature demands were quantified based on a uniform cross section of the bridge deck resulting in the majority of longitudinal cycles within 5-20% of the design displacement of the bearing. Finally, earthquake loading produced the highest amplitude bearing displacements.

This study extends the framework from Noade and Becker (2019) but investigates the effects of uncertainty and nonlinear behavior from aging by incorporating effects of corrosion on the bridge deck and piers. Furthermore, multiple bridge types are explored. Two common superstructure types are investigated, a precast concrete girder type and a slab on steel girder deck type, and variation in the numbers of bridge spans is also considered. Monte-Carlo simulation is used to account for variations in model parameters, effects of aging, and bridge demands. The findings of this study help to identify which design properties of the bridge influence the bearing demands. These results can be used by researchers to develop a bearing fatigue load protocol which includes the impact of bridge corrosion over time.

2. BRIDGE DESIGNS AND MODELLING

2.1 BRIDGE DESIGNS AND VARIATIONS

The designs of the bridges that are modelled in this study are based on the Chemin des Dalles Bridge located in Trois Rivières, Quebec City. This example bridge is used in this study as all the dimensions and section properties of the bridge are available and specified in Tavares et al. (2013). The superstructure consists of three equal spans with a reinforced concrete slab deck and six V-Type precast concrete girders. The substructure consists of two piers, each with three circular reinforced concrete columns connected by a bent beam. Each reinforced pier has a cover depth of 50.8mm and fifteen 35.81mm diameter longitudinal reinforcing bars. As the effects of aging occur, the stiffness properties of the bridge elements will reduce over time.

Earthquake loading can also cause the bridge to undergo high displacements which means highly nonlinear behavior in addition to the reduced stiffness. This may be particularly true for the reinforcing piers which are expected to sustain high drifts over several cycles. Therefore, the bridge is modelled in OpenSees (McKenna et al. 2010) using nonlinear displacement based fiber beam elements for the slab deck and pier columns (Figure 3). Each fiber element has 5 integration points between nodes for the slab deck and piers. The bridge is then validated with the periods and

mode shapes specified by Tavares et al. (2013). The bridge deck is modelled as a grillage to be able to apply multi-lane vehicle loading.

Laminated elastomeric bearings are located at the abutments, directly below each of the six precast girders. The bearings' rotational stiffness properties are determined following the analytical formula for multilayer rubber bearings with rectangular cross sections (Konstantinidis and Kelly, 2011) (Appendix A). Reducing the thickness of the rubber layer and increasing the shape factor and second moment of area result in a higher rotational bearing stiffness. The stiffness in the vertical direction is modelled as a linear spring, and to represent the nonlinear behaviour experienced by bearings in shear, a bilinear model with low yield strength is used in the horizontal direction. CSA S6-14 (CSA, 2014) states that no uplift should occur in the bearing when the edge of the bearing is vertically displaced for up to 14 percent of the total rubber thickness. Bearing manufacturers specify the maximum allowable bearing rotation. For the bearings assumed in the study, bearing rotation is limited to 7 percent of the total rubber thickness divided by half the length of the bearing (Goodco, 2010). Pin connections are located between the deck and the bents at the two piers, they are modelled with zero rotational stiffness about the out of plane axis with all other degrees of freedom fixed.

Two-span and single-span bridges, shown in Figure 4, are designed based on the initial three span Chemin des Dalles model to investigate the impact of variation in bridge design on the bearing demands. A second deck type, slab on steel girders, is also considered with single, two and three spans. The steel girders are W1000x371

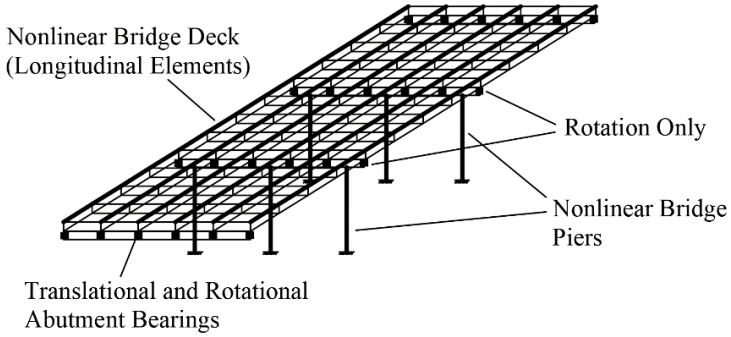

Figure 3. Nonlinear Opensees model of Chemin des Dalles Bridge

sections which are modelled using steel fiber displacement based elements. For each bridge model, the bearings are selected based on their governing longitudinal design displacements which are controlled by temperature. The steel girder bridge types have higher design displacements compared to the concrete girder bridges because of the higher thermal coefficient. In addition, the three span for both steel and concrete girder bridges has higher design displacements due to a larger expansion length than the two or one span. Table 1 lists the design displacements of the selected bearing and their stiffness properties for each of the bridge models. The first mode periods of the bridges are 0.43s, 0.45s, and 0.32s for the 3, 2, and 1 span concrete girder bridges, respectively. For the slab on steel girder bridges the

periods are 0.42s, 0.37s, and 0.33s respectively. The first mode of the 2 and 3 span bridges is transverse whereas the first mode for the 1 span bridges is vertical.

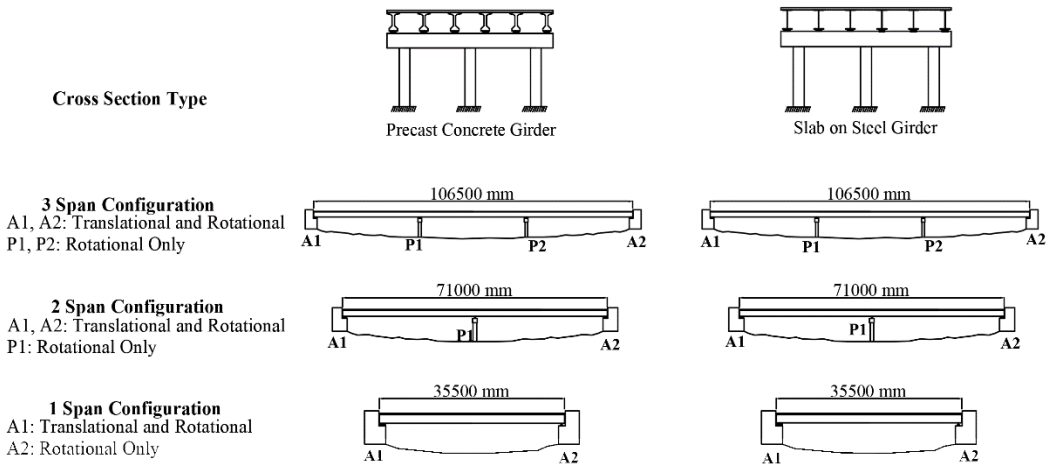

Figure 4. Bridge deck and span variation models

Table 1. Bearing properties for bridge design models

	Precast Concrete Girder Bridge		
Spans	3	2	1
Bearing (length x width x height)	400x300x75	400x300x60	400x300x60
Horizontal Stiffness (kN/mm)	2.39	3.28	3.28
Vertical Stiffness (kN/mm)	301.7	380.3	380.3
Rotational Stiffness (kNmm/rad)	45000	88140	88140
Longitudinal Design Disp. (mm)	22.6	15.1	15.1
Vertical Design Disp. (mm)	4.2	3.4	3.4
Rotational Design Limit (rad)	0.021	0.022	0.022
	Slab on Steel Girder Bridge		
Spans	3	2	1
Bearing (length x width x height)	400x300x90	400x300x70	400x300x70
Horizontal Stiffness (kN/mm)	2.00	2.63	2.63
Vertical Stiffness (kN/mm)	249.9	392.2	392.2
Rotational Stiffness (kNmm/rad)	26200	58600	58600
Longitudinal Design Disp. (mm)	29.4	19.6	19.6
Vertical Design Disp. (mm)	5.0	3.9	3.9
Rotational Design Limit (rad)	0.034	0.026	0.026

2.2 CORROSION OF REINFORCED CONCRETE MEMBERS

Corrosion in reinforced concrete bridges leads to reduction in rebar diameter as well as cracking and spalling of cover concrete in both the bridge deck and piers. To capture this, researchers have proposed time-dependent corrosion initiation and deterioration models. Early work on corrosion prediction led to the development of predictive models such as those proposed by Bazant (1979) and Morinaga (1988) which assume a linear propagation of corrosion. Stewart and Rosowsky (1998), and Kassir and Ghosn (2001) proposed models to calculate the time to corrosion initiation. These models are based on Fick's second law of diffusion, which represents the diffusion of chloride ions through the concrete. The chloride concentration *C* is expressed as

$$C(x,t) = C_s\left[1 - erf\left(\frac{x}{2\sqrt{Dt}}\right)\right] \quad (1)$$

where C_s is the chloride concentration at the surface, erf(.) is the error function, and D is the diffusion coefficient. The time to corrosion initiation T_{corr} (T_{cr} in Figure 1) is expressed as

$$T_{corr} = \frac{d^2}{4D}\frac{1}{\left[erf^{-1}\left(1-\frac{C_{cr}}{C_s}\right)\right]^2} \quad (2)$$

where *d* is the depth of cover and C_{cr} is the critical chloride concentration. Although corrosion can be localized, for modelling purposes corrosion is assumed to act uniformly along the length of the rebar member as suggested by Rao et al. (2017).

2.2.1 PIER CORROSION MODEL

The probabilistic model for reinforced concrete piers developed by DuraCrete (2000) and adopted by Choe et al. (2006) is used to find the corrosion initiation time. This model extends Equation 2 by considering uncertainties in the environmental condition of the bridge. The corrosion initiation time is calculated as

$$T_{corr} = X_1 \left[\frac{d^2}{4k_e k_t k_c D_0 (t_0)^n} \left[erf^{-1} \left(1 - \frac{C_{cr}}{C_s} \right) \right]^{-2} \right]^{1/(1-n)} \quad (3)$$

where X_1 is a model uncertainty coefficient, k_e is an environmental factor, k_t is a factor accounting for the influence of test methods to determine the diffusion coefficient, k_c is a factor for the influence of curing, D_0 and t_0 are the empirical diffusion coefficient and reference period to diffusion respectively, and n is an age factor. Cover depth and water-cement ratio, *w/c* are critical parameters (Vu and Stewart 2000), where higher water- cement ratio and less cover lead to earlier corrosion initiation times and increased rates of corrosion. The water-cement ratio of the Chemin des Dalles Bridge is unknown, and therefore it is treated as a uniform random variable (Table 2). All other factors are treated as discrete variables based on their mean values from the experimental testing undertaken by DuraCrete (2000) and shown in Table 3.

The corrosion propagation model used for the reinforced concrete piers is based on the nonlinear corrosion rate function model developed by Vu and Stewart (2000)

and adopted by other researchers, such as Choe et al. (2006) and Kumar and Gardoni (2008). The reinforcement reduction with time is estimated as

$$d_b(t, T_{corr}) = \begin{cases} d_{bi} & t \le T_{corr} \\ d_b(t) = d_{bi} - \frac{1.0508\left(1-\frac{w}{c}\right)^{-1.64}}{d}(t - T_{corr})^{0.71} & T_{corr} \le t \le T_f \\ 0 & t > T_f \end{cases} \quad (4)$$

where $d_b(t,T_{corr})$ is the reduced bar diameter at time t given the known corrosion initiation time T_{corr}, the initial bar diameter d_{bi}, and the water-cement ratio w/c. T_f is the theoretical time when the bar diameter is fully corroded. However, the value of T_f is much larger than the lifespan of the bridge being considered hence the longitudinal reinforcement never reaches full corrosion.

2.2.2 DECK CORROSION MODEL

Equation 2 is used to determine the corrosion initiation time for the bridge deck. The time to corrosion initiation is more variable and can occur sooner in decks than in piers. For regions with cold temperatures, this can be due to deicing salts during winter months which cause varying levels of surface chloride concentrations. Therefore, the surface chloride concentration, C_s is assumed to be uniformly distributed between the low and high concentrations used by Kassir and Ghosn (2001) and specified in Table 2. In addition, the diffusivity of ions can vary for different decks, therefore the diffusion coefficient D is also treated as uniformly distributed (Table 2).

Equation 4 is used to determine the diameter of reinforcement corrosion. The cover depth and water-cement ratio are not known for the Chemin des Dalles bridge deck. Therefore, the cover depth is treated as a uniform distribution based on the cover depth tolerances specified in CSA S6-14 (2014), and the water cement ratio is uniformly distributed with the same tolerances outlined in the pier corrosion model (Table 2).

During corrosion, the expansion of rust at the steel concrete interface will result in cover cracking and spalling of concrete. Coronelli and Gambarova (2004) proposed a simplified method to incorporate the effect of cover spalling and cracking by reducing the unconfined strength of the cover concrete which is applied to the reinforced concrete piers and the bridge deck.

Table 2. Random variables for concrete corrosion model

	Reinforced Concrete Piers		**Reference**
	Distribution Type	Value	
Water-Cement Ratio $\frac{w}{c}$	Uniform	0.4 - 0.5	(Choe et al. 2006, CSA S6-14 2014)

	Reinforced Concrete Slab Deck		**Reference**
Surface Chloride Concentration C_s	Uniform	23.27 - 69.82 N/m³	(Kassir and Ghosn, 2001)
Diffusion Coefficient D	Uniform	39.5 - 131.6 mm²/yr	(Kassir and Ghosn, 2001)
Cover Depth d	Uniform	45 - 55 mm	(CSA S6-14 2014)
Water-Cement Ratio $\frac{w}{c}$	Uniform	0.4 - 0.5	(Choe et al. 2006, S6 CSA 2014)

Table 3. Pier corrosion model parameters based on mean values

Pier Corrosion Model Parameters			
Coefficient	Mean Value	Coefficient	Mean Value
X_1	1.000	k_c	0.8
k_e	0.676	D_0	220.9 - 473 (linearly interpolated based on *w/c*)
k_t	0.832	t_0	28 days
n	0.362		

2.3 CORROSION OF STEEL MEMBERS

The slab on steel girder bridge models include corrosion of the reinforced concrete slab deck and piers. In addition, the steel girders are susceptible to atmospheric corrosion which causes a uniform thickness reduction of the steel members with time. Localized corrosion such as pitting corrosion is also common and can often be seen to occur at the ends of the girder where parts of the bridge are exposed to moisture leakage and debris. A sensitivity analysis was conducted by reducing the thickness properties of the steel at the girder ends by up to three times the amount expected for uniform corrosion. This caused negligible change to the bearing demand, and therefore localized corrosion is neglected from this study. Jiang et al. (2000) adopted a power law for uniform corrosion of the steel based on the work by Keyser and Nowak (1989), where the steel corrosion is calculated as

$$C(t) = At^B \tag{5}$$

where A and B are parameters both related to the type of environment and steel type, and $C(t)$ is the average corrosion penetration. A and B are treated as random variables (Table 4) with mean and standard deviation based on the values given by

Keyser and Nowak (1989) for an urban environment. Further, carbon steel is assumed as corrosion is more detrimental to this steel type compared to weathering steel.

Table 4. Random variables for steel corrosion model

	Urban Environment (normal distribution assumed)	
	A ($x10^{-6}$ m)	B
Mean, μ	80.2	0.593
Standard Deviation, σ	0.42	0.400

2.4 CHANGE IN STIFFNESS DUE TO CORROSION

Corrosion of the concrete girder and the slab on steel girder bridges causes the flexural stiffness of the bridge deck and piers to reduce over time. Over 70 years, the flexural stiffness of the concrete girder and slab on steel bridge decks is expected to decrease on the order of 16% (11.9 kN/mm at t = 0 years) and 18% (8.93 kN/mm at t = 0 years) respectively for the bridge designs considered. For the bridge substructure, the flexural stiffness decreases by less than 2% after 70 years. The stiffness reduction for the substructure is much lower than deck because the piers have a high cover depth, large diameter of longitudinal reinforcement, and lower chloride concentrations.

3. METHODOLOGY

Thermal, traffic, and seismic are the primary load types considered for this study. Monte Carlo simulations (Metropolis and Ulam, 1949) are carried out at four ages in the bridge life span, i.e., at t = 10, 30, 50, and 70 years. These selected ages each represent a 20-year span. Thus, for each load type (temperature, seismic, traffic), the annual demands are quantified at age t and then multiplied by 20 to represent the demands for a period range of 20 years. Given no prior research for a period range, a value of 20 years is assumed in this study. For each Monte Carlo simulation, random variables, listed in Table 2 and Table 4, are generated for the corrosion parameters, resulting in an initial deteriorated condition for the loading. The random variables used in determining the loading are given in Table *5*. For each excitation, the rainflow cycle counting method (ASTM 1997, FEMA 2007) is used to quantify the number of bearing cycles for specified ranges of the design displacement of the bearing (Noade and Becker, 2019).

Table 5. Random variables for bridge loading

	Temperature Loading	
	Distribution Type	Value
Selection of Uniform Temperature Data	50 years of day/night temperatures	
Temperature Differential, ΔT for each month	Normal	Mean: Figure 3 Coefficient of Variation: 0.1
	Seismic Loading	
Selection of Earthquake Ground Motion	15 ground motions	
	Traffic Loading	
Total Number of Daily Trucks	Uniform	550 – 672 trucks

3.1 TEMPERATURE LOADING

Daily temperature fluctuations cause the bridge deck to expand and contract resulting in bearing displacement predominantly in the longitudinal direction because of uniformity in the cross section of the deck and the large expansion length. However, there is also rotational demand created by vertical thermal gradients over the depth of the deck. There is often a temperature variation through the depth of the deck's cross section. For example, when the top surface of deck is warmer than the soffit, there is a positive thermal gradient. Positive gradients are expected to occur during the warmest hours in the afternoon, and negative gradients at cooler temperatures during early hours of the morning. The temperature difference ΔT between the top surface of the deck and deck soffit results in a bending moment in the deck that causes rotational and longitudinal displacement of the bearings and is calculated as

$$M = \frac{EI\alpha\Delta T}{h} \tag{6}$$

where EI is the bending rigidity of the deck, α is the coefficient of thermal expansion, and h is the depth of the deck. Hedegaard and French (2013) observed that strong positive thermal gradients were most prominent during summer months whereas negative gradients were more consistent throughout the year, and concluded that design thermal gradients are not necessarily conservative because of factors such as the locality of the bridge as well as variations in the material

behavior of the deck which can significantly influence the temperature gradient and cause it to exceed the design gradient.

CSA S6-14 (2014) specifies the temperature differential for concrete girder bridges for both summer and winter conditions. Given the depth of the deck's cross section CSA S6-14 (2014) gives a 10˚C summer positive and 5˚C winter positive or negative temperature differential. CSA S6-14 (2014) specifies bridges with steel systems and concrete decks as Type B. Vertical temperature differentials only exist in the reinforcing slab but not in the steel girder for Type B superstructures. CSA S6-14 (2014) only considers positive temperature differentials for Type B superstructures, neglecting negative differentials. Kennedy and Soliman (1987) proposed recommended maximum values for the temperature differential which occur in the reinforcing slab for slab on steel girder bridges. The positive differential values are given as 22.2˚C during the summer and 11.1˚C during winter, and a 4.2˚C negative differential to occur over the entire year. Interpolating for the months between summer and winter, the values of ΔT over the year are shown in Figure 5. Considering that the temperature differential is uncertain and may exceed the design code limits, the value of ΔT for each month is assumed as a random variable with a mean equal to the value shown in Figure 5 and a coefficient of variation (CoV) of 0.1 (Nowak and Collins, 2000) given in Table 5.

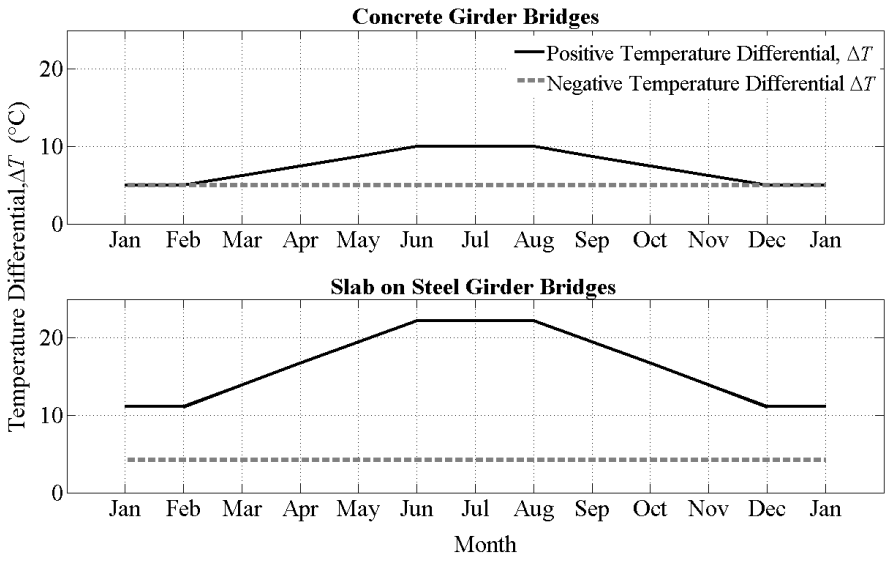

Figure 5. Positive and negative temperature differential variation for concrete girder bridge and slab on steel girder bridge for a single year

For analysis, a corroded bridge model is generated through Monte Carlo sampling. For the uniform temperature change, causing expansion and contraction of the deck, a single year of day and night temperature data is selected from 50-years of recorded data available for Quebec City available from Environment Canada (2017). The day and night temperatures are converted to applied longitudinal displacements of the bridge deck. For the thermal gradient across the deck, corresponding daytime (positive thermal gradient) and night time (negative thermal gradient) values of ΔT are generated using the mean and CoV values for each month. Using Equation 6, the temperature differentials are converted to applied moments and applied together with the longitudinal displacements of the bridge deck. Rainflow cycle counting is then used to determine the annual number of cycles and displacements of the bearing.

3.2 SEISMIC LOADING

This study uses fifteen synthetic ground motions for Eastern North America (Atkinson 2009) which were scaled by Noade and Becker (2019) for Quebec City site class C at three hazard levels of 2%, 10%, and 40% probability of exceedance in 50 years (Figure 6). For each simulation run in the Monte Carlo analysis for the earthquake loading, a single three-component ground motion is selected along with a corrosive condition of the bridge. The Monte Carlo analysis is conducted for each hazard level and at time intervals *t*. Each simulation output produces a displacement history response of the bearing. The numbers of cycles and displacement amplitudes are found for each hazard level. The annual demands are found by multiplying by the ranges of the annual rate of exceedance for each hazard level and summing over the hazard levels (Noade and Becker, 2019).

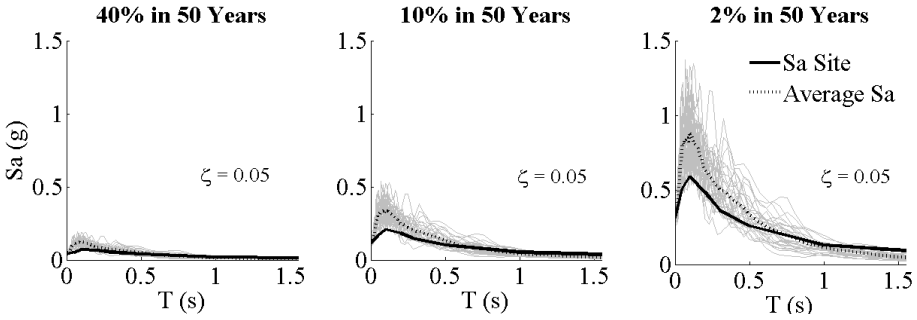

Figure 6. Scaled time histories at 3 hazard levels for Quebec City

3.3 TRAFFIC LOADING

This study considers the CL-625 truck load type (CSA S6-14 2014), i.e., the heaviest vehicle loading over the bridge according to Canadian standards. Five

scenarios (Figure 7) are used to represent possible truck loading on the bridge. Scenarios 1 and 2 are single trucks loaded in each direction. Scenarios 3 and 4 consider two trucks per lane loaded in each direction with a truck spacing of 60 m, which is the minimum spacing distance as outlined by MTO (2019). Scenario 5 considers trucks loaded on opposite lanes of the bridge. Scenarios which include a single truck only are likely to occur during periods of the day when traffic is low, (e.g., during night hours). Other scenarios are more common during peak traffic hours. The resulting expected percentage of loading for each scenario is given in Table *6*.

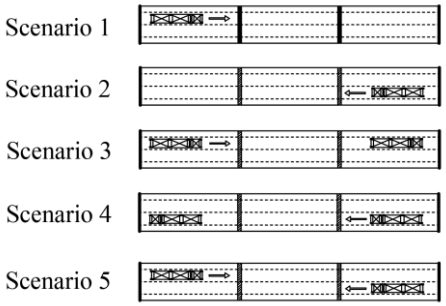

Figure 7. Five single and multi-truck loading scenarios over highway bridge

Table 6. Expected occurrence of truck loading scenarios per day

Scenario	Expected Occurrence Per Day (%)
1	25
2	25
3	15
4	15
5	20

Monte Carlo simulation is used to account for uncertainties in the number of trucks per day and the distribution between the loading scenarios. The number of trucks

per day is assumed as uniformly distributed with a 10 percent variation on the 611 daily expected trucks used by Noade and Becker (2019). Each scenario is independently analysed to determine the demands on the bridge bearing in terms of number of cycles and cycle amplitudes in the longitudinal, vertical, and rotational directions. To find the demands over a given day, the expected number of trucks is chosen from a uniform distribution. Then the trucks are distributed between the five loading scenarios using a Monte Carlo simulation, based on the probabilities shown in Table *6*. A corroded bridge model is generated and loaded from which the expected number of cycles and cycle amplitudes of the bearing per day are determined.

3.4 NUMBER OF SIMULATION TRIALS

An initial estimation of the number of simulation runs for each load type is described by Oberle (2015) which is based on the central limit theorem

$$n = \left(\frac{z_{1/2}\,\sigma}{\Delta}\right)^2 \tag{7}$$

where $z_{1/2}$ is the confidence interval, σ is the standard deviation and Δ is the margin of error. A small sample size of 30 simulation trials is used to determine the value of standard deviation, and a confidence level of 5% is selected to find the expected value for the loading demands. Using Equation 7, the initial estimation of the number of simulations required is 41, 73 and 133 runs for the temperature, seismic and traffic loading respectively for the 1 span concrete girder bridge at t = 10 years.

To check these required number of simulation runs is sufficient, the number of expected cycles are plotted against the number of simulation runs until convergence is achieved (i.e. by conducting a sensitivity analysis about the required number of Monte Carlo trials for each *t*). Figure 8 shows the expected number of longitudinal cycles of the bearing for each amplitude range for the 3 load types for the 1 span concrete girder bridge and the number of simulation trials for the other bridge types. Appendix B shows the convergence test at the 3 other periods, *t* for the 1 span concrete girder bridge. The same was checked for the different bridge models and at different periods, *t.* As more simulation trials are generated, the number of expected cycles converge for each amplitude range. Table 7 presents the number of simulation trials carried out for each load type at the four periods, *t* for the 1 span concrete girder bridge.

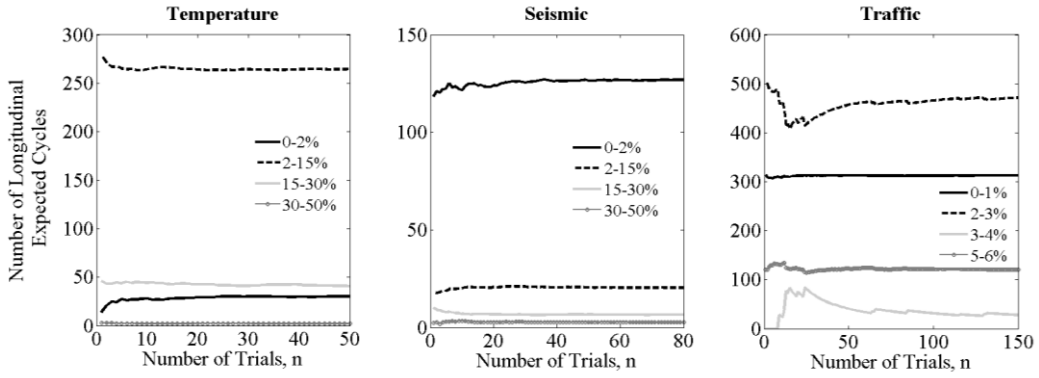

Figure 8. Number of simulation trials required at t = 10 years for longitudinal direction of 1 span concrete girder bridge

Table 7. Number of Monte Carlo simulation trials carried out for 1 span concrete girder bridge for all loadings

Load Type	Number of simulation trials, n			
	t = 10 years	t = 30 years	t = 50 years	t = 70 years
Temperature	50	70	90	110
Seismic	80	120	160	200
Traffic	150	170	200	220

4. LIFETIME BEARING DEMANDS

The bearing demands are presented in terms of the percentage of design displacement values listed in Table 1 for ease of comparison between bridge types (Figure 4). The demands are separated into four 20-year time periods. For each time period, the number of cycles and bearing displacements are determined. The number of cycles are then distributed into displacement bins, representing a range of the displacement amplitude of the bearing. As traffic loading produces significantly lower longitudinal displacements compared to seismic and temperature, smaller bin ranges are used for these loads.

4.1 TEMPERATURE DEMANDS

The bearing demands due to temperature loading for the concrete girder bridges and steel girder bridges in the longitudinal direction are presented in Figure 9. The amplitudes and cycles of the bearing are consistent in the longitudinal direction for all of the bridge designs and demands remain below 50% of the design displacement. This is because the bearings were initially selected by finding the expected longitudinal thermal movement based on the bridge material and location. The bearing movement in the longitudinal direction is primarily due to the uniform thermal load. The thermal gradient contributes significantly less to the longitudinal movement, but causes the bearing to rotate at the same time the longitudinal displacements occur. Aging of the bridge does not affect the longitudinal demands as shown in Figure *9*. Expansion and contraction of the bridge deck does not cause

bending in the deck and causes little demand in the bridge piers because of the bearings; thus, deterioration of the deck and piers have negligible influence on the thermal bearing demands.

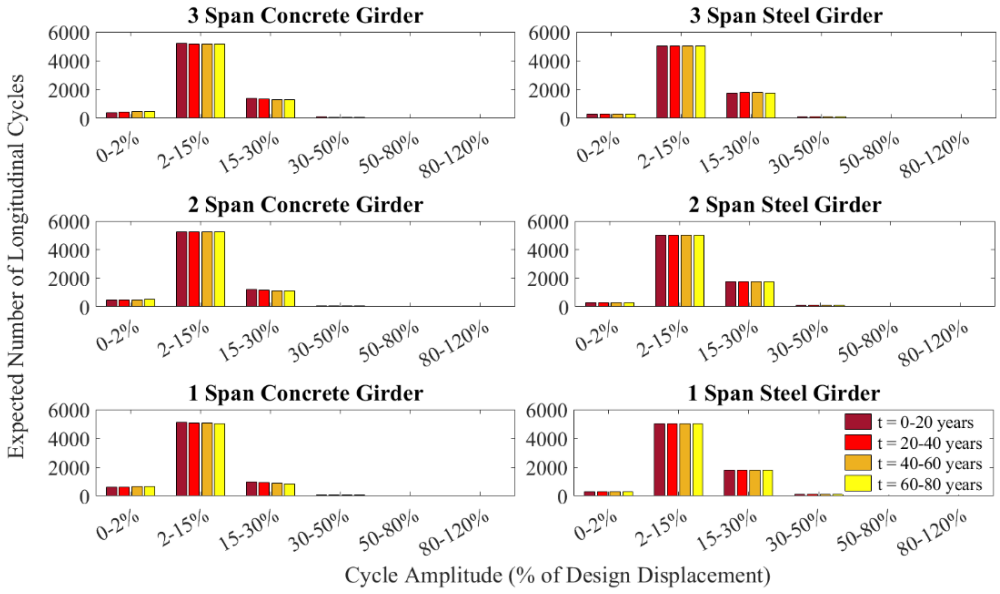

Figure 9. Expected longitudinal bearing cycles due to temperature loading over 20 year age ranges

The rotational bearing demands due to thermal loading for the concrete girder bridge designs are presented in Table 8. Thermal gradients cause rotations at the bearings. For the concrete girder bridges the rotational bearing demands are less than 5% of the design rotation, while the slab on steel girder bridges have all cycles within 0-2% of the design rotation. The smaller demands in the steel girder bridges is because the temperature gradient occurs only in the slab deck, while for the concrete girder bridges, the temperature gradient is throughout the depth of the cross section. As the rotations from the thermal gradients are small to begin with,

there is minimal change with aging, and the amplitudes increased by less than 2% over the lifespan of the concrete girder bridges.

Table 8. Rotational bearing cyclic demands due to temperature loading for concrete girder bridges over 20 year spans

Design Displacement Range (%)	0-20 Years	20-40 Years	40-60 Years	60-80 Years
3 Span Concrete Girder Bridge				
0-2	7202	6828	6260	5578
2-5	67	441	1009	1692
2 Span Concrete Girder Bridge				
0-2	7252	7188	7004	6710
2-5	19	81	267	560
1 Span Concrete Girder Bridge				
0-2	6986	6198	5220	4170
2-5	284	1073	2050	3100

4.2 SEISMIC DEMANDS

The expected number of longitudinal cycles due to seismic loading over 20 year intervals are separated into seven amplitude bins (Figure 10). There is a significant variation in the demands between the number of bridge spans. The single span bridges have the highest number of bearing cycles in the 0-2% amplitude range. The 2 and 3 span bridges have large bearing displacements that exceed the design displacements; however, the bearings have design displacements at 50% strain and can reach much larger displacements before damage. The single span bridges have no piers, resulting in a larger longitudinal stiffness, leading to high numbers of cycles with low displacement amplitudes. The 2 and 3 span bridges have similar stiffness resulting in similar demands, although the additional pier in the 3 span

bridges results in a slightly lower period and therefore more cycles at lower displacements compared to the 2 span bridges.

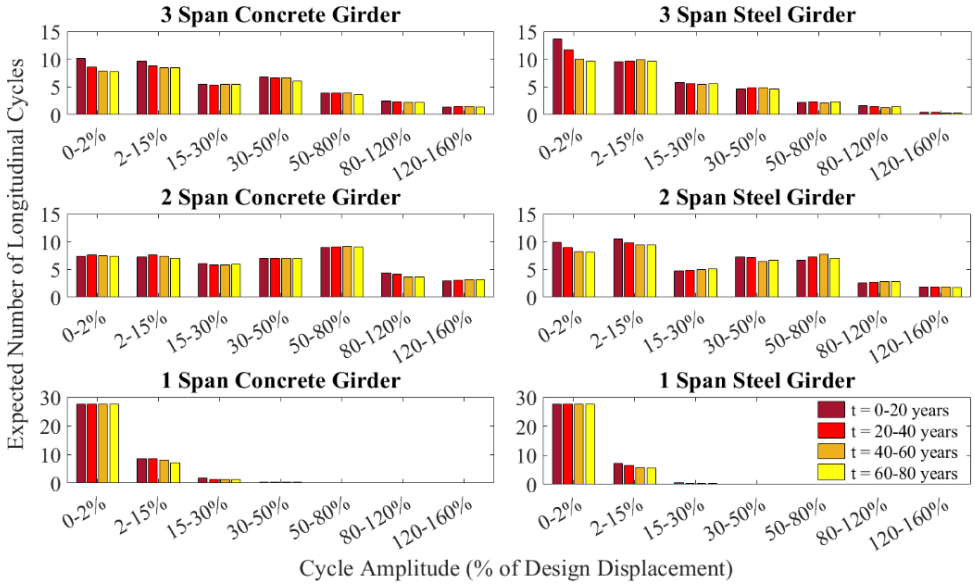

Figure 10. Expected longitudinal bearing cycles due to seismic loading over 20 year spans

Overall aging results in negligible change to the demand in the bearing for both concrete and steel girder bridges. A reduced bridge stiffness causes the period to elongate and thus larger overall displacements are expected; however, more of this displacement is accommodated in the pier. For the 2 and 3 span bridges, there is a noticeable decrease in the number of expected cycles within the 0-2% amplitude range as the bridge ages. This is due to reduction in the pier strength leading to yielding and hysteretic energy dissipation, reducing low amplitude cycles.

Figure 11 shows the vertical and rotational bearing demands for the concrete girder bridges due to seismic loading. These very low demands are similar for the slab on

steel girder bridges (Appendix C). For all bridge models, over 80% of the vertical and rotational cycles fall below 2% of the design displacement. The bearings are stiff in the vertical direction and also the vertical intensity of the synthetic earthquake ground motions for Quebec City used in this study is relatively low, resulting in small vertical displacement demands. In addition, the rotational stiffness properties of the bearings are high leading to low overall rotational displacements. Aging results in negligible change to the longitudinal demands as the piers have minimal reduction in the flexural stiffness due to aging.

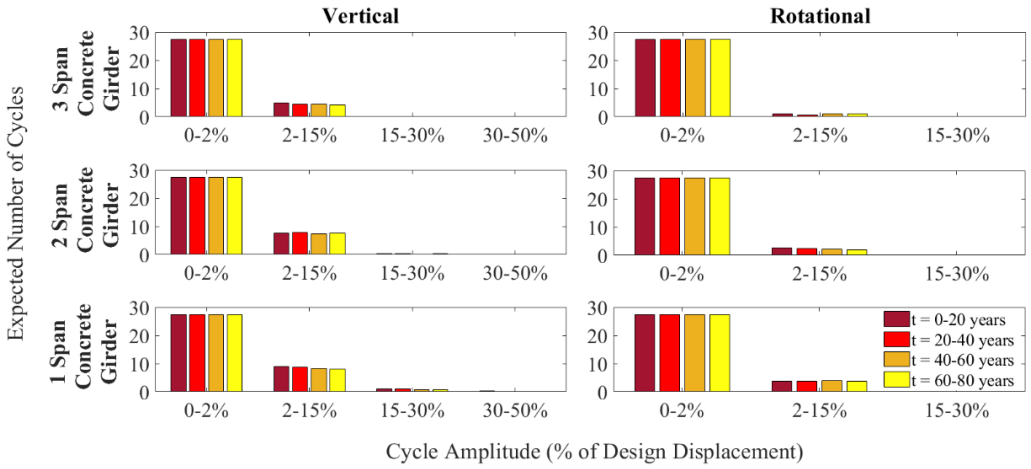

Figure 11. Expected vertical and rotational bearing cycles for concrete girder bridges due to seismic loading over 20 year spans

4.3 TRAFFIC DEMANDS

Displacement history plots for the truck loading scenarios are shown in Figure 12 for the concrete girder deck bridges, and the expected longitudinal cycles are shown in Figure 13. Similar displacement histories are observed for the steel bridges

(Appendix D). Scenario 3 and 4 (Figure 7) are excluded from the 1 and 2 span bridges because these bridges are not long enough to accommodate two trucks with the minimum truck clearance. For all loading scenarios, increasing the number of bridge spans reduces the longitudinal bearing displacement demands. Longitudinal bearing displacements are caused by the bending of the bridge deck. For the same span length, the bending of the deck is reduced for bridges with larger number of spans due to hogging moments developed at the pin supports, reducing the longitudinal bearing displacement. However, increasing the number of spans will result in more longitudinal cycles because the truck causes the deck to bend as it moves over adjacent spans of the bridge. Increasing the number of spans results in a minimal change in the peak vertical bearing displacement because the vertical load is kept the same and the selected bearings all have a high vertical stiffness in each of the bridge models.

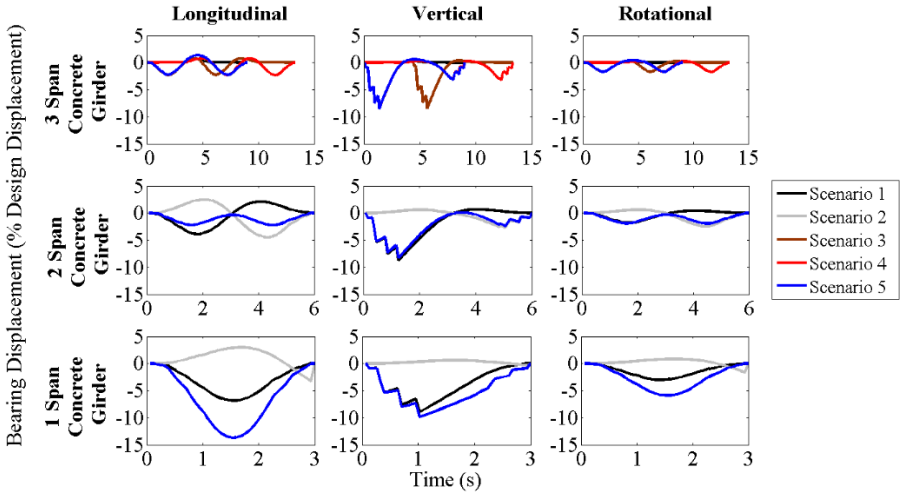

Figure 12. Displacement histories of traffic load scenarios for concrete girder deck bridge

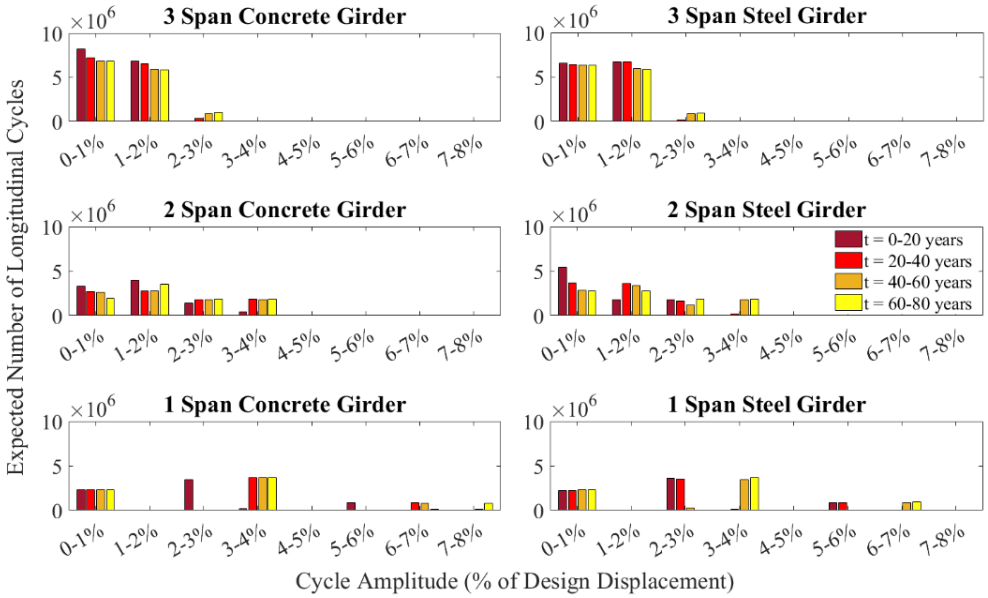

Figure 13. Expected longitudinal bearing cycles due to traffic loading over 20 year spans

The impact of bridge aging on traffic demands is shown in Figure 14. The displacement histories in the longitudinal and vertical directions are presented at t = 10 and t = 70 years for the loading scenario 1. Bridge aging causes a small increase in the longitudinal bearing displacement. The displacement histories have a maximum increase of less than 2% of the bearing design displacement for the 1 span bridge between t = 10 and t = 70 years. The increase in displacement demand is caused due to a more flexible deck which will have larger bending. However, the vertical demands have negligible change with age because aging of the bridge deck is independent of the vertical bearing load.

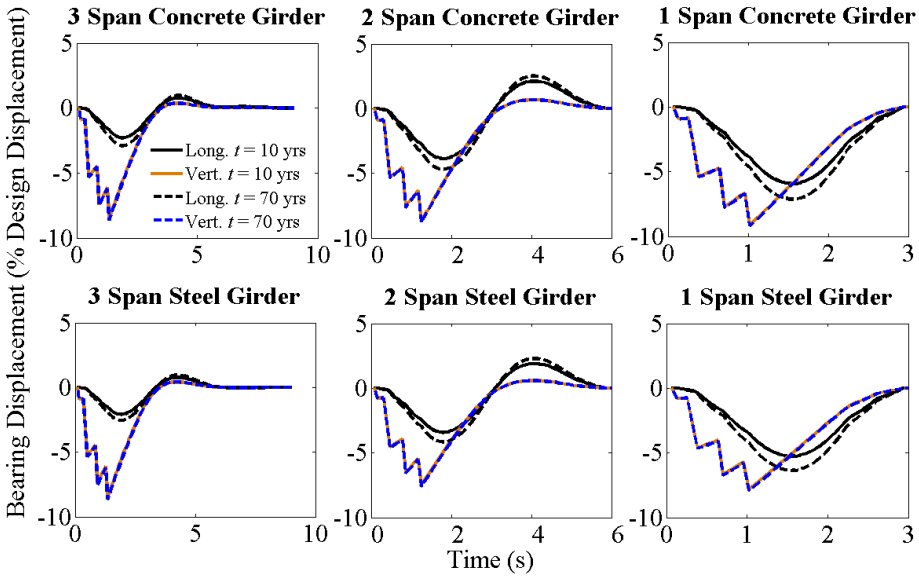

Figure 14. Displacement histories in the longitudinal and vertical directions for traffic load scenario 1 for all bridge designs at time t = 10 and t = 70 years

5. COMPARISON OF DEMANDS

Figure 15 shows the total expected number of cycles for each bridge design due to the three load types over 80 years. Seismic loading has a negligible number of cycles, with traffic loading dominating the cyclic demands. This is also true in all directions of loading.

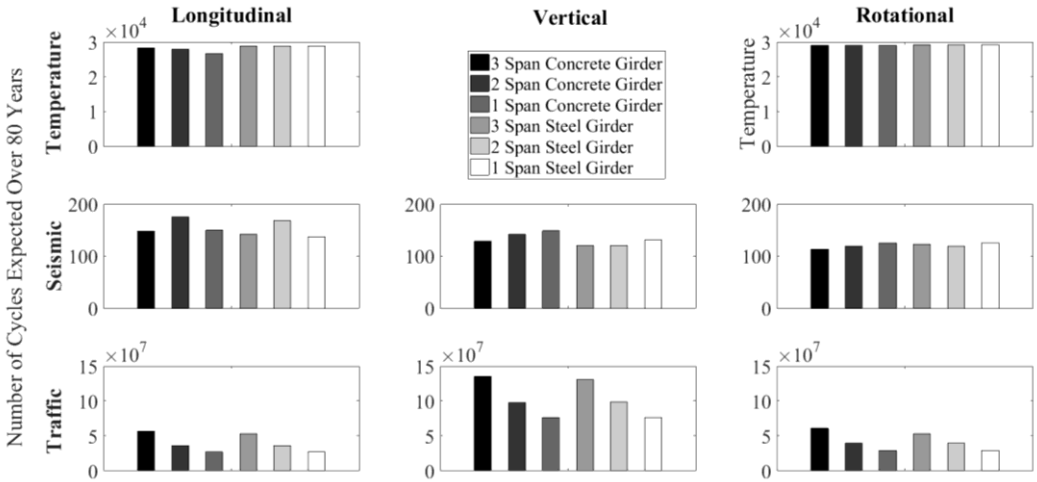

Figure 15. Expected number of bearing cycles over 80 years for the three load types in the longitudinal, vertical, and rotational directions for all bridge designs

Although bridge aging has very little impact on the displacement amplitudes, the lifetime loading can be significantly affected. This is particularly true for traffic loading as the bearing experiences the largest number of cycles for this load type. The total annual distance travelled by the bearing under traffic loading increases by 33.5%, 35.6%, and 2.28% from t = 10 to t = 70 years in the longitudinal direction for the 1, 2, and 3 span concrete girder bridges, respectively. The cumulative rotation travel increases by 26.8%, 32.3%, and 63.9% from t = 10 years to t = 70

years for the 1, 2, and 3 span concrete girder bridges, respectively. Similar increases were found for the steel girder bridges. The effect of aging on lifetime traffic demands is further evident in Figure 16 which shows the cumulative distance travelled by the bearing in the three degrees of freedom due to traffic loading. The nonlinear increase in the longitudinal and rotational demands means that there is increased displacement demand with aging. In the vertical direction, the demands increase is constant as aging has no impact on the demands in this direction.

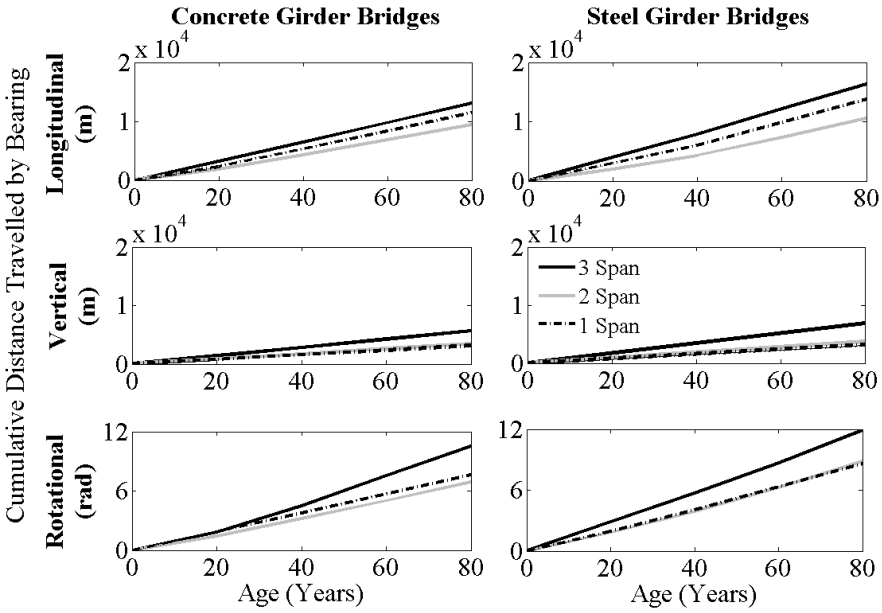

Figure 16. Expected cumulative distance travelled by the bearing in the longitudinal, vertical, and rotational directions for traffic loading for all bridge designs

The number of bridge spans has a larger influence on bearing demands than the type of deck. For seismic loading, the amplitude of the longitudinal displacements for the 1 span are significantly smaller compared to the 2 and 3 span bridges because

of the difference in stiffness. For thermal loading, the longitudinal bearing demands are similar for all bridge designs even though the longitudinal design displacements are different. This is because the bearings are initially selected based on the governing thermal movement in the longitudinal direction. Therefore, by finding the expected maximum bearing displacement, an appropriate bearing selection is made such that the demands can be limited to 50% of the bearings design displacement for each of the bridge types. For traffic loading, increasing the number of spans increases the number of longitudinal, vertical, and rotational bearing cycles (Figure 15). However, although the 2 span bridges undergo more cycles than the 1 span (Figure 15), the 1 span bridges experience more longitudinal wear of the bearing after a period of 80 years (Figure 16). This is because the 1 span bridges have higher amplitude cycles compared to the 2 span bridges (Figure 13).

Figure 17 presents the cumulative longitudinal distance travelled by the bearing from all load types divided into displacement amplitude ranges for the concrete girder bridges. The distances for the bearings in the steel girder bridges are slightly larger, similar to what is seen in Figure 16. Again, the traffic loading dominates the total displacement demand with contributions from low amplitude loading, temperature fluctuations account for midrange displacements, and seismic demands account for rare larger displacement demands.

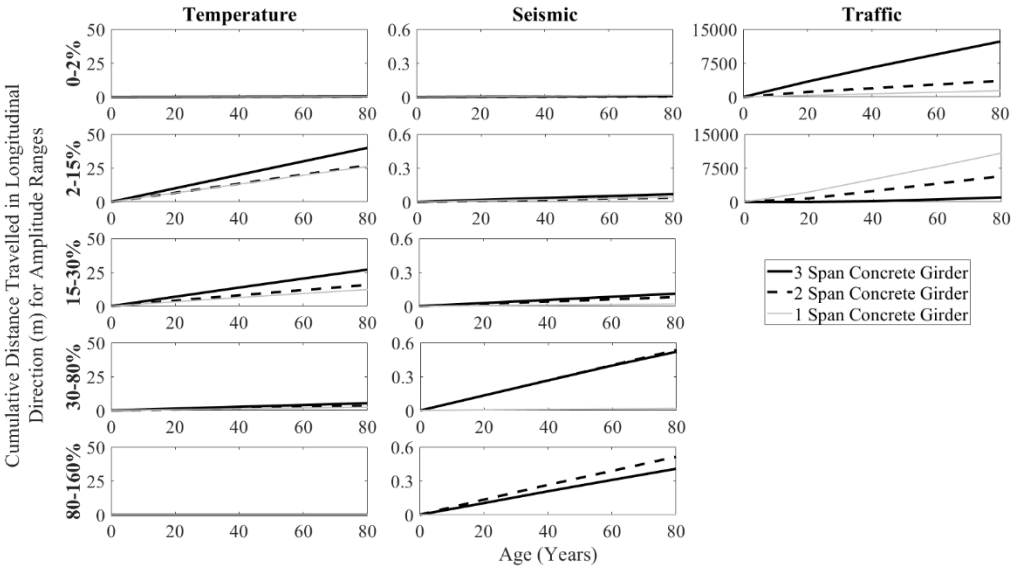

Figure 17. Expected cumulative longitudinal distance travelled by bearing for temperature, seismic and traffic loading for concrete girder bridges

6. CONCLUSIONS

This study investigates the effects of aging and bridge design on lifetime bridge bearing demands for three primary load types: temperature due to a uniform temperature change and vertical thermal gradient, seismic events and daily traffic. Two types of superstructures, concrete girder and steel girder, and three different numbers of spans are used. Bridge aging is taken account through corrosion prediction models which reduce the longitudinal reinforcement diameter and consider spalling of cover concrete. For the steel girder bridges, this also includes uniform corrosion of the steel girders. Monte Carlo simulation was used to account for uncertainty in the deterioration and loading.

Overall, bridge aging results in very small increases of the displacement demands of the bearing for the load types considered. Aging increased the rotational displacements due to thermal loading by 2% and had little impact on the longitudinal displacement demands. For seismic loading, bridge aging did not have any major impact; however, at very low displacements the number of cycles reduced with aging due to yielding from strength reduction resulting in hysteretic damping. Finally, longitudinal and rotational demands due to traffic loading increased by less than 2% after 80 years of aging. However, given the large number of cycles due to traffic loading, this results in a significant effect on the lifetime travel of the bearings.

More spans resulted in an increased number of expected cycles. However, the 1 span bridges had more longitudinal wear of the bearing than the 2 span bridges over the service life of the bridge. This occurred because the 1 span bridges have smaller numbers of cycles but at higher displacement amplitudes compared to the 2 span bridges which can significantly add to the longitudinal travel of the bearing.

Compared to the other designs, the 3 span bridge undergoes the largest number of bearing cycles, and travels the largest distances. Also, due to seismic loading, the bearing displaces to high amplitudes which exceed the design displacement for several cycles in the longitudinal direction in the case of the 2 and 3 span bridges.

Using these bearing demands fatigue load protocols can be developed for the experimental testing of laminated elastomeric bridge bearings in the longitudinal, vertical and rotational degrees of freedom.

7. RECOMMENDATIONS FOR FUTURE WORK

7.1 MODEL DEVELOPMENT

In this study, several bridge models were developed to investigate the differences between bridge bearing demands by varying the deck type and the numbers of spans of the bridge. As the number of spans of the bridge was found to be the most influential design parameter, future work could include a variation on the length of bridge spans. In addition, this study only considered the use of elastomeric type bearings and alternative bearing articulations with pot and sliding type bearings could also be introduced.

The results of this study showed the effect of corrosion due to aging increased the longitudinal wear of the bearing significantly for traffic loading. Therefore, sensitivities in the traffic loading and its impact on long term longitudinal, vertical and rotational wear should be investigated further. Development of the traffic scenarios to include traffic accumulation on the bridge and standstill traffic should be considered. Also load variation can be integrated into the model by applying probabilistic distributions for vehicle loading.

During seismic events the bridge piers can endure large displacements resulting in inelastic deformations. Damage from inelastic deformations can cause the stiffness

of the piers to decrease, even though the bridge itself still remains serviceable. Future work can incorporate the effects of low cycle fatigue in the modelling, and explore multiple earthquake events over the bridges' lifespan.

7.2 BEARING LOAD PROTOCOL

The demands presented in this study can be used to develop a fatigue load protocol for reinforced elastomeric bridge bearings to experimentally investigate bearing degradation over its service life. The vertical, longitudinal and rotational demands have been summarized here, and therefore future development of a load protocol could include simultaneous loading in each of these three degrees of freedom to represent realistic demands that are typically experienced by bearings in practice. This study quantified bearing demands into four 20- year periods to determine the effect of bridge aging on changes to demands. For this reason, a proposed load protocol can incorporate the impact of aging by applying the loading in 4 stages, with each stage representing the demands for a single 20-year period.

8. REFERENCES

ASCE. 2017. Infrastructure Report Card. Accessed July 2019. Retrieved from https://www.infrastructurereportcard.org/cat-item/bridges/

ASTM. 1997. Standard Practice for Cycle Counting in Fatigue Analysis. E 1049-85. West Conshohocken, PA: ASTM.

Atkinson, G. M. 2009. Earthquake time histories compatible with the 2005 National building code of Canada uniform hazard spectrum. Canadian Journal of Civil Engineering, 36 (6):991-1000.

Bazant, Z. P. 1979. Physical model for steel corrosion in concrete sea structures-application. Journal of the. Structural Division. 105 (6):1155-1166.

CSA (Canadian Standards Association). 2014a. Canadian Highway Bridge Design Code. CSA S6-14. Toronto:CSA.

Choe, D., P. Gardoni., D. Rosowsky., and T. Haukaas. 2007. Probabilistic capacity models and seismic fragility estimates for RC columns subject to corrosion. Reliability Engineering and System Safety, 93 (3):383-393.

Cohen J. M., and V. Wetzk. 2016. Failures of US bridge rocker bearings. Proceedings of the Institution of Civil Engineers – Engineering History and Heritage, 169 (3):123-129.

Coronelli D., and P. Gambarova. 2004. Structural assessment of corroded reinforced concrete beams: modelling guidelines. Journal of Structural Engineering, 130 (8):1214-1224.

DuraCrete. 2000. Statistical quantification of the variables in the limit state functions. The European Union Brite EuRam 3 contract BRPR-CT95-0132 Project BE95-1347 Report no BE95-1347/R7 May 2000.

Government of Canada. 2017. Historical Data. Accessed November 2018. Retrieved from http://climate.weather.gc.ca/

FEMA. 2007. Interim Testing Protocols for determining the seismic performance characteristics of structural and nonstructural components. FEMA 461. Washington, DC: FEMA.

Goodco Z-Tech. 2010. Elastomeric bearings [Brochure]. Québec: Canam Group Inc.

Grata, J. 2008. Birmingham Bridge Report Confirms Rocker Bearing Failure. Accessed September 2019. Retrieved from https://www.post-gazette.com/breaking/2008/07/01/Birmingham-Bridge-report-confirms-rocker-bearing-failure/stories/200807010159

Hedegaard, B., and C. French. 2013. Investigation of thermal gradient effects in the I-35W St. Anthony Falls Bridge. Journal of Bridge Engineering, 18 (9):890-900.

Jiang, M., R. Corotis., and J. Ellis. 2000. Optimal life-cycle costing with partial observability. Journal of Infrastructure Systems, 6 (2):56-66.

Kassir M. K., and M. Ghosn. 2001. Chloride-induced corrosion of reinforced concrete bridge decks. Cement and Concrete Research, 32 (1):139-143.

Kayser J. R., and A. Nowak. 1989. Reliability of corroded steel girder bridges. Structural Safety, 6(1): 53-63.

Kelly J. M., and D. Konstantinidis. 2011. Mechanics of rubber bearings for seismic and vibration isolation. A John Wiley & Sons, Ltd.

Kennedy J.B., and M.H. Soliman. 1987. Temperature distribution in composite bridges. Journal of Structural Engineering, 113 (3): 475-482.

Kumar, R., P. Gardoni., and M. Sanchez-Silva. 2008. Effect of cumulative seismic damage and corrosion on the life-cycle cost of reinforced concrete bridges. Earthquake Engineering Structural Dynamics, 38 (7): 887-905.

McKenna, F., M.H. Scott., and G.L. Fenves. 2010. Nonlinear finite element analysis software architecture using object composition. Journal of Computing in Civil Engineering, 24 (1):95-107.

Metropolis, N., and S. Ulam. 1949. The Monte Carlo method. Journal of the American Statistical Association, 44 (247):335-341.

Ministry of Transportation Ontario. 2019. The Official MTO Truck Handbook. Accessed January 2019. Retrieved from http://www.mto.gov.on.ca/english/trucks/handbook/index.shtml

Morinaga, S. 1988. Prediction of service lives of reinforced concrete buildings based on rate of corrosion of reinforcing steel. Report No. 23. Shimizu Corp, Japan, pp. 82-89.

Noade B. M., and T.C. Becker. 2019. A probabilistic framework for lifetime bridge bering demands. Journal of Bridge Engineering. 24(7): 04019065.

Noury P., and K. Eriksson. 2017. Failures of high strength stainless steel bridge roller bearings: A review. Engineering Fracture Mechanics, 180: 315-329.

Nowak, A.S, and K.R. Collins. 2000. Reliability of structures. McGraw-Hill, New York, USA.

Oberle, W. F. 2015. Monte Carlo Simulations: Number of iterations and accuracy. Accessed August 2018. Retrieved from https://www.semanticscholar.org/paper/Monte-Carlo-Simulations%3A-Number-of-Iterations-and-Oberle/8c0f562de271a9be324f9abbfdc68c78b0d33f65

O'Flaherty, F.J., P.S. Mangat., and P. Lambert. 2010. Influence of steel reinforcement corrosion on the stiffness of simply supported concrete beams. Bridge Maintenance, Safety, Management and Life-Cycle Optimization, IABMAS' 10, July 11-15 2010, Philadelphia, PA, USA.

Rao, A.S., M.D. Lepech., A.S. Kiremidjian., and X.Y. Sun. 2017. Simplified structural deterioration model for reinforced concrete bridge piers under cyclic loading. Structure and Infrastructure Engineering, 13 (1):55-66.

Roeder, C.W., J.F. Stanton., and A.W. Taylor. 1990. Fatigue of steel reinforced elastomeric bearings. Journal of Structural Engineering. 116 (2):407-426.

Stewart M.G., and D.V. Rosowsky. 1998. Structural safety and serviceability of concrete bridges subject to corrosion. Journal of Infrastructure Systems, 4 (4):146-155.

Tavares D.H., J.R. Suescun., P. Paultre., and J.E. Padgett. 2013. Seismic fragility of highway bridge in Quebec. Journal of Bridge Engineering, 18 (11):1131-1139.

Taylor P., and A. Brooks. 2013. Specifying structural steel for bridges. Construction Canada. Accessed September 2019. Retrieved from https://www.constructioncanada.net/specifying-structural-steel-for-bridges/

Torres-Acosta, A.A., M.J. Fabela-Gallegos., A. Muñoz-Noval., D. Vázquez-Vega., J.R. Hernandez-Jimenez., and M. Martínez-Madrid. 2004. Influence of corrosion on the structural stiffness of reinforced concrete beams. Corrosion Engineering, 60 (9):862-872.

Vu K., and M. Stewart. 2000. Structural reliability of concrete bridges including improved chloride-induced corrosion models. Structural Safety, 22 (4):313-333.

Warn G.P., and P. Deng. 2016. Modelling the compression stiffness degradation in circular elastomeric bearings due to fatigue. Journal of Engineering Mechanics, 142(1): 04015057-1.

Yakut A., and J.A. Yura. 2002. Evaluation of elastomeric bearing performance at low temperatures. Journal of Structural Engineering, 128(8): 986-994.

Zhou Y., B. Gencturk., K. William., and A. Attar. 2014. Carbonation-induced and chloride-induced corrosion in reinforced concrete structures. Journal of Materials in Civil Engineering, 27(9): 04014245-1.

APPENDIX A

Bending Stiffness for Multi-Layer Rubber Bearings under Bending (Konstantinidis and Kelly, 2011):

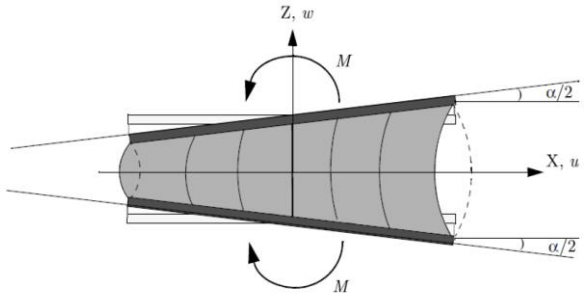

α is the angle between the rigid plates
t is the thickness of the rubber layer
$M / \alpha = (EI)_{eff} / t$ where $M / \alpha = k_r$ or the rotational bearing stiffness

APPENDIX B

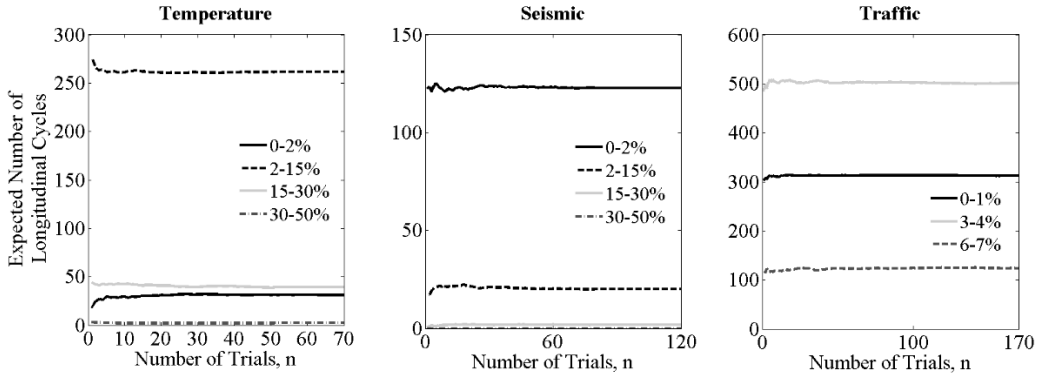

Number of simulation trials required at t = 30 years for longitudinal direction of 1 span concrete girder bridge

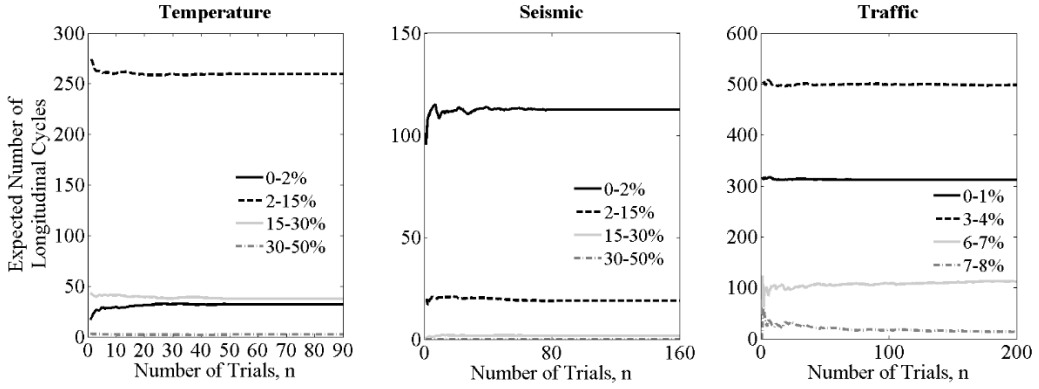

Number of simulation trials required at t = 50 years for longitudinal direction of 1 span concrete girder bridge

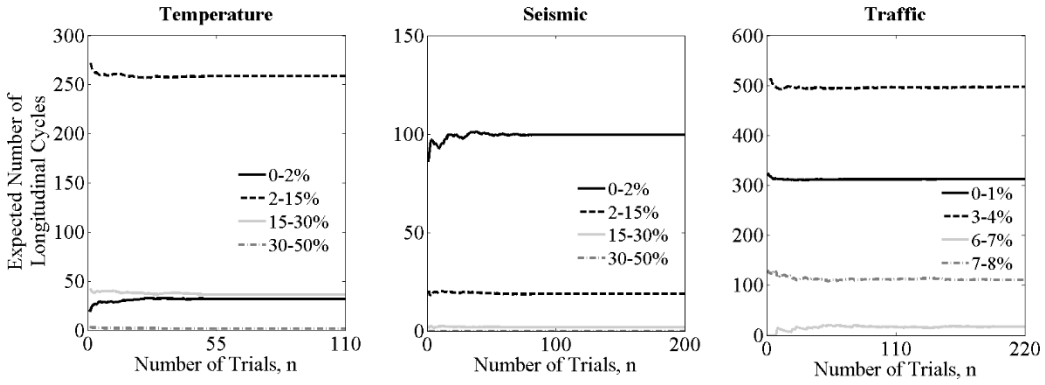

Number of simulation trials required at t = 70 years for longitudinal direction of 1 span concrete girder bridge

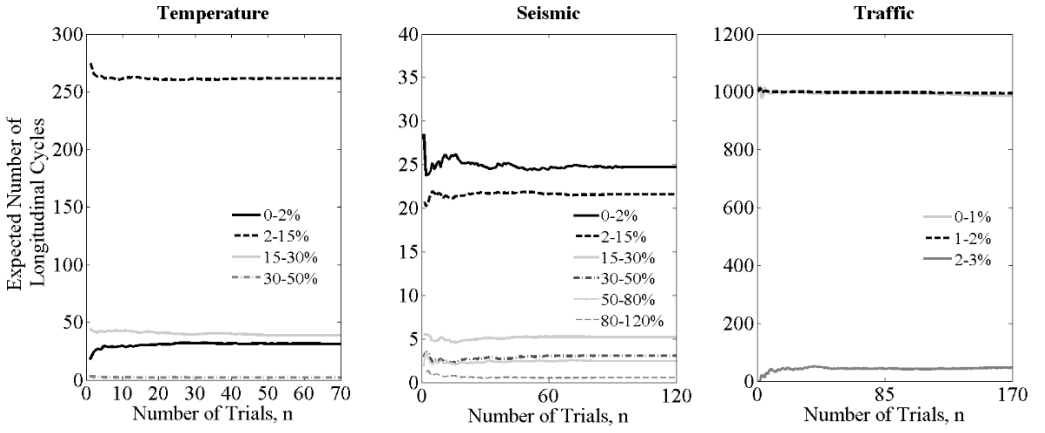

Number of simulation trials required at t = 30 years for longitudinal direction of 3 span concrete girder bridge

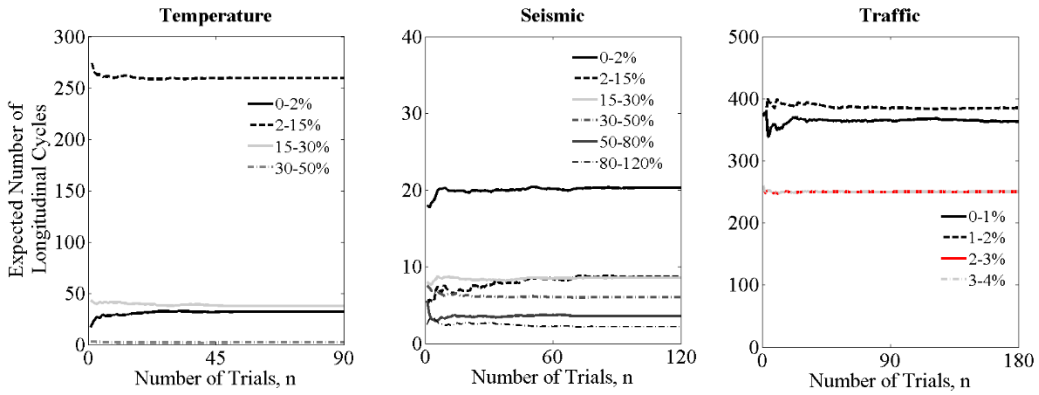

Number of simulation trials required at t = 50 years for longitudinal direction of 2 span concrete girder bridge

Table A. Number of simulation trials for 3 span and 2 span concrete girder bridges

Load Type	Number of simulation trials, n			
	3 Span Concrete Girder Bridge			
	t = 10 years	t = 30 years	t = 50 years	t = 70 years
Temperature	50	70	90	110
Seismic	80	120	160	200
Traffic	150	170	180	200
	2 Span Concrete Girder Bridge			
Temperature	50	70	90	110
Seismic	80	120	160	200
Traffic	150	170	180	200

Table B. Number of simulation trials for steel girder bridges

Load Type	Number of simulation trials, n			
	3 Span Steel Girder Bridge			
	t = 10 years	t = 30 years	t = 50 years	t = 70 years
Temperature	50	70	90	110
Seismic	80	120	160	200
Traffic	150	170	190	200
	2 Span Steel Girder Bridge			
Temperature	50	70	90	110
Seismic	80	120	160	200
Traffic	150	170	180	200
	1 Span Steel Girder Bridge			
Temperature	50	70	90	110
Seismic	80	120	160	200
Traffic	150	180	220	250

APPENDIX C

Table A. Vertical bearing cycles due to seismic loading for slab on steel girder bridges at periods, *t*

Design Displacement Range (%)	0-20 Years	20-40 Years	40-60 Years	60-80 Years
	3 Span Steel Girder Bridge			
0-2	27.5	27.5	27.5	27.5
2-15	3.13	2.62	2.56	2.64
	2 Span Steel Girder Bridge			
0-2	27.5	27.5	27.5	27.5
2-15	2.63	2.76	2.75	2.73
	1 Span Steel Girder Bridge			
0-2	27.5	27.5	27.5	27.5
2-15	6.28	5.44	4.95	4.69
15-30	0.12	0.08	0.06	0.04

Table B. Rotational bearing cycles due to seismic loading for slab on steel girder bridges at periods, *t*

Design Displacement Range (%)	0-20 Years	20-40 Years	40-60 Years	60-80 Years
	3 Span Steel Girder Bridge			
0-2	27.5	27.5	27.5	27.5
2-15	1.01	1.01	1.01	1.01
	2 Span Steel Girder Bridge			
0-2	27.5	27.5	27.5	27.5
2-15	2.13	2.21	2.15	2.37
	1 Span Steel Girder Bridge			
0-2	27.5	27.5	27.5	27.5
2-15	4.18	3.86	3.77	3.65
15-30	0.02	0.02	0.02	0.02

APPENDIX D

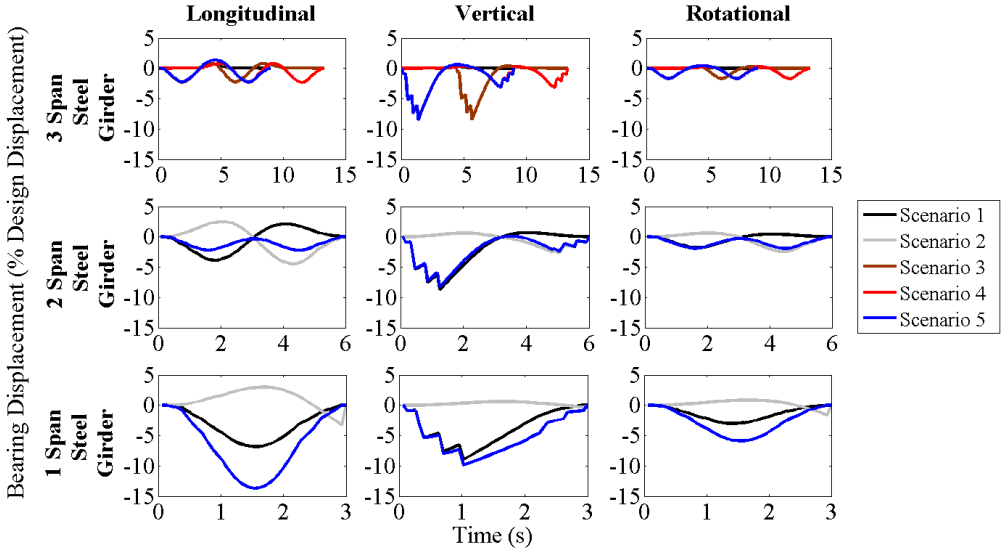

Figure A. Displacement histories of traffic load scenarios for steel girder deck bridge